Eco-engineered bio-based palladium MOF chitosan–carboxymethyl cellulose composite sponge: mechanistic insights, Box–Behnken optimization, and high-performance reusability for advanced ciprofloxacin removal from wastewater

Table S1. Chemical name, formula, and company

Chemical name	Formula	Company
Chitosan	$C_{56}H_{103}N_9O_3$	Sigma-Aldrich, Germany
Carboxymethyl cellulose		Sigma-Aldrich, Germany
Itaconic acid	$C_5H_6O_4$	Sigma-Aldrich, Germany
1,3,5-Tricarboxylic benzene	$C_9H_6O_6$	Sigma-Aldrich, Germany
Palladium (II) nitrate dihydrate	$Pd(NO_3)_2.2H_2O$	Sigma-Aldrich, Germany
N,N-Dimethylformamide (DMF)	C_3H_7NO	Sigma-Aldrich, Germany
Methanol	CH_3OH	LOBA CHEMIE PVT.LTD, India
Ethanol	C_2H_5OH	Sigma-Aldrich, Germany
Sodium hydroxide (99%, AR)	NaOH	Chimmed, Russia
Hydrochloric acid (37%, AR)	HCl	LOBA CHEMIE PVT.LTD, India

Table S2. Instruments and equibments.

Test name	Abbrevation	Instrument name	Company	Illustration
Fourier transformer infrared	FT-IR	A Nicolet IS10 Fourier transform infrared (FTIR) spectrometer	Thermo Fisher Scientific, Waltham, MA, USA	equipped with an attenuated total reflectance accessory and which ran in the 4000-400 cm^{-1} range was used to gather FTIR spectra
Powered X-ray diffraction	PXRD	Siemens diffractometer (model D500, Germany)	Germany	patterns were captured from powder samples through the use of a Siemens diffractometer (model D500, Germany) that was fitted with a Cu-K radiation source (wavelength 1.54 Angstroms (Å)) operating at 30 kV and 20 mA.
Scanning Electron Microscope	SEM	(JSM-6510LV, JEOL Ltd., Tokyo, Japan)	JEOL Ltd., Tokyo, Japan	The morphology of the investigated sorbents was analyzed with the use of a scanning electron microscope
X-ray photoelectron spectroscopy	XPS	K-ALPHA (Themo Fisher Scientific, USA)	Themo Fisher Scientific, USA	Used for determination the elemental analysis for the compound
Brunauer–Emmett–Teller	BET	Quantachrome Instruments, Anton Paar Quanta Tec, Inc., Boynton Beach, FL,	Quanta Tec, Inc., Boynton Beach, FL, USA	was utilised for surface and pore analysis (Brunauer–Emmett–Teller) (BET) surface area, porous volume, and pore size), and NovaWin Software (v11.0) was used for data interpretation.

		USA		The BET surface area of material adsorbents was obtained by the application of nitrogen adsorption-desorption isotherms at 77K through the use of a specific analyser (Quadrasorb–EVO, Quantachrome, USA).
UV-visible spectrophotometer	UV spectrophotometer	Jasco V-630	Japan	Measuring the concentration of the adsorbate soulution via using Bear-Lambert law
Energy Dispersive X-ray	EDX	Leo1430VP microscope	Carl Zeiss AG, Jena, Germany	Elemntal analysis of the material
Transmission electron microscopy	TEM	TEM, FEI Teanci G2 F20, USA	FEI Teanci G2 F20, USA	Determination the morphology of the material and size
pH meter	pH	HANNA (model 211)	USA	Measuring the acidity or basicity of the solution
Sonication	Ultrasonic	Elmasonic P300H ultrasonic bath, continuous mode, power 380 W	Elma Schmidbauer GmbH, Singen, Germany	Sonication of the material as well as used ton disperse material on the solution as it decrease the particle size of the material
Water bath	Shaking	GFL Orbital Shaker 3017		
Atomic	atomic absorption spectrometer	SIMAA 6000		Determination metal concentration

Table S3. True variables, codes, and their BBD levels.

Code	Variables	-1	0	+1
A	pH	2	5	8
B	Dose (g)	0.02	0.25	0.5
C	Time (min.)	5	55.5	100

Table S4. A detailed analysis of the CIP absorption and surface interactions within the central composite structure is essential for accurate assessment.

Run	Real variables			Yield (mmol/g)		
	pH	Time (min.)	Dose (g)	Investigational	Predicted	Residue
1	6.5	52.5	0.26	295.121	295.12	0.0000
2	10	52.5	0.5	201.93	198.19	3.74
3	6.5	100	0.02	481.412	454.21	27.20
4	3	52.5	0.02	239.786	243.52	-3.74
5	3	52.5	0.5	182.694	178.26	4.44
6	6.5	5	0.5	23.7649	50.97	-27.20
7	10	52.5	0.02	306.926	311.36	-4.44
8	10	5	0.26	26.223	2.76	23.46
9	6.5	52.5	0.26	295.121	295.12	0.0000
10	6.5	100	0.5	300.882	281.86	19.03
11	6.5	52.5	0.26	295.121	295.12	0.0000
12	6.5	52.5	0.26	295.121	295.12	0.0000
13	6.5	52.5	0.26	295.121	295.12	0.0000
14	3	100	0.26	249.436	272.90	-23.46
15	6.5	5	0.02	38.0239	57.05	-19.03
16	3	5	0.26	19.7015	-3.06	22.76
17	10	100	0.26	332.083	354.85	-22.76

Table S5. BET surface area and pore volume parameters.

Sample	BET Surface Area (m^2/g)	Total Pore Volume (cm^3/g)	Notes
PMCC	87.56	0.12	Mesoporous structure with broad pore distribution.
CIP@PMCC	68.60	0.088	Decrease indicates pore filling and partial blockage after CIP adsorption.

Table S6. Pore radius and Pore size distribution.

Sample	Main Pore Radius (nm)	Pore Size Distribution Range (nm)	Interpretation
PMCC	2.34	2–4 (main peak); tail up to ~20	Well-defined mesoporous structure.
CIP@PMCC	1.96	Shift toward smaller pores	Indicates partial pore blockage by CIP.

Table S7. Elemental analysis of PMCC and CIP@PMCC.

Element	PMCC	CIP@PMCC
C1s	32.91	28.16
N1s	36	34.78
O1s	16.09	14.46
Pd3d	15	12.80
F	-	9.80

Table S8. Equations used in this work to fit the data of adsorption experiments.

Serial	Equation	Nmae	Description	Ref.
1	$q_e = \frac{q_m}{1 + K_L C_e}$	Langmuir	q_e (mg.g^{-1}) Adsorption capacity, C_e equilibrium concentration, q_m (mg.g^{-1}) is the monolayer saturation capacity constant and K_L (L/mg) is the Langmuir constant associated with the free adsorption energy. The favorability of the adsorption process in the Langmuir model is determined by means of the R_L dimensionless factor ($R_L = 1/(1 + k_L \cdot C_0)$) as follows: $R_L = 0$, $0 < R_L < 1$, $R_L = 1$, and $R_L > 1$ indicating irreversible, favorable, linear, and unfavorable adsorption isotherms, respectively.	[1]
2	$q_e = K_F C_e^{\frac{1}{n}}$	Freundlich	K_F Freundlich isotherm constants [(mg/g)/(mg/L)$^{1/n}$], and $1/n$ represents the exponent of non-linearity (i.e., C-type, L-type, and S-type isotherms). n is the Freundlich constants, and $n < 1$ indicates poor adsorption while $n = 1$–2 and $n = 2$–10 indicate average and good adsorptions, respectively. The values of n and k_f are calculated, respectively	[2]
3	$q_e = q_m \exp(-\beta\varepsilon^2)$ $\varepsilon = RT ln\left(1 + \frac{1}{C_e}\right)$ $E_{DR} = \sqrt{\frac{1}{2K_{DR}}}$	Dubinin–Radushkevich	q_D is the maximum monolayer adsorption capacity (mg/g), B_D is the activity coefficient related to the apparent free energy of adsorbate adsorption onto the adsorbent (mol^2/kJ^2), ε_D is the Polanyi potential which is related to the equilibrium concentration, and E is the mean adsorption energy.	[3]
4	$q_e = Q_{max} \frac{RT}{b} \ln(K_T C_e)$	Temkin	K_T is the Temkin isotherm constant or equilibrium binding constant (L/mg) corresponding to the maximum binding energy, and b_T is the Temkin isotherm constant related to the heat of adsorbate adsorption onto the adsorbent due to adsorbent-adsorbate interaction (J/mol), R is the gas constant (8.314 J/mol/K), and T is the absolute temperature (herein 298 K).	[4]

	$q_e = \frac{q_m k_T c_e}{(1 + (K_L C_e)t)1/t}$	Toth	q_e: amount of adsorbate adsorbed at equilibrium (mg/g), Ce:equilibrium concentration of adsorbate in solution (mg/L) q_{max}: theoretical maximum adsorption capacity (mg/g) K_T: Toth isotherm constant related to affinity (L/mg) t t: heterogeneity parameter (dimensionless)	[5]
5	$q_t = q_e\left(1 - e^{K_1 t}\right)$	Pseudo-First-order kinetic	q_e and q_t are the adsorption capacities at equilibrium and time t (mg/g), and k_1 is the rate constant (min^{-1}), respectively.	[6]
6	$q_t = \frac{tK_2 q_e^2}{1 + q_e K_2 t}$	Pseudo-Second-order kinetic	k_2 is the pseudo-second order constant (mg/(g.min))	[7]
7	$q_t = K_i t^{1/2} + X$	Intraparticle diffusion	q_t is the adsorption capacity at time t in (mg/g), k_{int} is the intraparticle diffusion rate constant ($mg \cdot g^{-1} \cdot min^{-1/2}$), and C is a constant related to the the thickness of the boundary layer (mg/g).	[8]
8	$q_t = \frac{1}{\beta}\ln(\alpha\beta t + 1)$	Elovich	The constants α chemical adsorption rate ($mg.g^{-1}min^{-1}$), and β Coefficient in relation with extension of covered surface	[9]
9	$\Delta G^o = \Delta H^o - T\Delta S^o$	Gibbs free energy	ΔG°: Gibbs free energy change; Kd: equilibrium constant; R: gas constant; T: temperature.	[10]
10	$LnK_d = \frac{\Delta S^\circ}{R} - \frac{\Delta H^\circ}{RT}$	Van't Hoff	ΔS°: entropy change; ΔH°: enthalpy change.	[11]
11	$LnK_d = lnA - (\frac{Ea^0}{R})\frac{1}{T}$	Arhinus	Ea was the activation energy, A Arhinus constant, R ideal gas constant 8.314 J/mol K, T (K) is the absolute solution temperature	[12]

Table S9. List of abbreviation.

Symbol	Definition
q_e	the adsorbed amount of dye at equilibrium concentration ($mg.g^{-1}$)
q_{mL}	the maximum sorption capacity (corresponding to the saturation of the monolayer, ($mg.g^{-1}$)
K_L	Langmuir binding constant which is related to the energy of sorption (L/mg)
C_e	is the equilibrium concentration of dyes in solution
K_F	Freundlich constants related to the sorption capacity (mg/g) $(L/mg)^{1/n}$
n	intensity
K_{DR}	constant related to the sorption energy (mol^2kJ^{-2})
q_{DR}	theoretical saturation capacity (mg/g)
ε	Polanyi potential (J^2mol^{-2})
R	Gas constant (8.314 $J.mol^{-1}K^{-1}$)
T	temperature where the adsorption occurs
A_T	Temkin isotherm constant
b_T	Temkin constant in relation to heat of adsorption ($J.mol^{-1}$)
q_t	is the amount of dye adsorbed ($mmol.g^{-1}$)
K_1	Rate constant for Pseudo first order constant for the adsorption processes (min^{-1})
q_2	Maximum adsorption capacity for pseudo second order
K_2	Rate constant for Pseudo first order constant for the adsorption processes ($g.mg^{-1}min^{-1}$)
α	Chemical adsorption rate ($mg.g^{-1}min^{-1}$)
β	Coefficient in relation with extension of covered surface
ΔG^o	Free Gibb's energy
ΔH^o	Enthalpy
ΔS^o	Entropy
K_c	distribution coefficient
C_{eq}	Concentration at equilibrium (mg/L)

Table S10. The parameter of the adsorption isotherm for CIP on PMCC composite sponge.

Isotherm	Value of parameters	
Langmuir	$q_{m\ exp}$ (mg/g)	480.5
	q_m (mg/g)	482.6
	K_L (L/mg)	0.034
	R_L	0.115
	Reduced Chi-Sqr	274.12101
	Residual Sum of Squares	4385.93611
	R-Square (COD)	0.98889
	R^2	0.9882
Freundlich	n	2.811
	K_F (mg/g) $(L/mg)^{1/n}$	78.39
	Reduced Chi-Sqr	1554.33491
	Residual Sum of Squares	24869.35861
	R-Square (COD)	0.93702
	R^2	0.93308
Dubinin–Radushkevich	$Q_{DR}(mg.g^{-1})$	423.2604
	K_{DR} ($mol^2k\ J^{-2}$)	7.14307E-6
	Ea (kJ/mol)	33.6
	Reduced Chi-Sqr	2987.99789
	Residual Sum of Squares	47807.96627
	R-Square (COD)	0.87892
	R^2	0.87135
Temkin	b_T (J/mol)	20.92
	K_T (L/mol)	0.35
	Reduced Chi-Sqr	346.31202
	Residual Sum of Squares	5540.99226
	R-Square (COD)	0.98597
	R^2	0.98509
Jossens	K	17.89994

	J	0.02732
	Reduced Chi-Sqr	286.49721
	Residual Sum of Squares	4297.4581
	R-Square (COD)	0.98912
	R^2	0.98766
Toth	q_m	536.30
	K_T (L/mg)	43.89
	t	1.102
	Reduced Chi-Sqr	285.2944
	Residual Sum of Squares	4279.41606
	R-Square (COD)	0.98916
	R^2	0.98772

Table S11. Models of adsorption kinetic parameters of CIP on PMCC composite sponge.

Model	Value of parameters	
Pseudo-First-order kinetic	K_1 (min^{-1})x10^{-2}	0.01684
	Reduced Chi-Sqr	6.56068
	Residual Sum of Squares	6547.56094
	R-Square (COD)	0.99964
	R^2	0.99964
Pseudo-second-order kinetic	K_2 (g $mg^{-1}min^{-1}$)x10^{-2}	1.2798E-5
	q_e (mg/g)	484.6
	Reduced Chi-Sqr	19
	Residual Sum of Squares	283.24749
	R-Square (COD)	5381.70232
	R^2	0.98932
Intraparticle diffusion	K_i ($mg.g^{-1}min^{1/2}$)	48.994
	X (mg/g)	70.22
	Reduced Chi-Sqr	1482.45007

	Residual Sum of Squares	29649.00134
	R-Square (COD)	0.94119
	R^2	0.94119
Elovich	β (g/mg)	175.576
	α ($mg.g^{-1}min^{-1}$)	8.92358E-4
	Reduced Chi-Sqr	752.17391
	Residual Sum of Squares	14291.30437
	R-Square (COD)	0.97165
	R^2	0.97016
Experimental data	q_e (exp) (mmol/g)	481.42

Table S12. The thermodynamic parameters.

T (K)	ΔG° (kJ/mol)	ΔH° (kJ/mol)	ΔS° (J/mol.K)
293	-1.15057		
298	-2.72649	91.2	315.2
303	-4.30241		
308	-5.87833		
313	-7.45425		
318	-9.03017		

Table S13. Comparison of adsorbent adsorption capacity of antibiotics.

Material	Q_{max}(mg/g)	References
P-CNT3	28.6	[13]
resin-based activated carbon	384.8	[14]
GO	354.24	[15]
chitosan-CNT	23.7	[16]

ZnCo-ZIF@CS	348.9	[17]
Fe/N-BC	46.45	[18]
MSCA	440.1	[19]
Fe/Ni-MOF	232.1	[20]
Modified cellulose adsorbent	150	[21]
Chitosan/GO composite	282.9	[22]
PMCC	480.5	This search

Table S14. The total of squared variances for the subsequent models.

Source	Sum of Squares	df	Mean Square	Sequential p-value	Adjusted R^2	Predicted R^2	
Linear	57357.91	9	6373.10	0.0001	0.7427	0.6412	
2FI	48423.98	6	8070.66	0.6208	0.7176	0.4209	
Quadratic	4408.65	3	1469.55	0.0005	0.9633	0.7429	Suggested
Cubic	0.0000	0			1.0000		Aliased

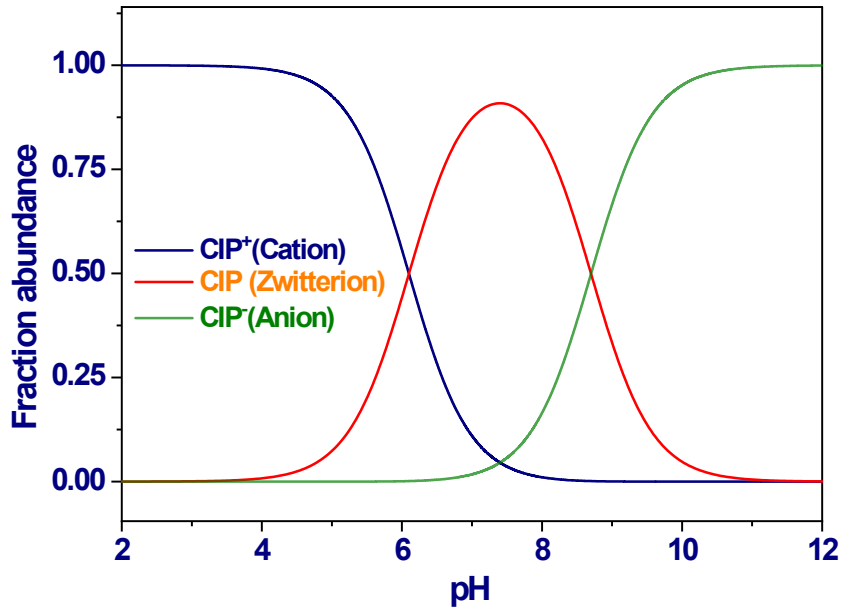

Fig. S1. pH dependent speciation of ciprofloxacin (CIP).

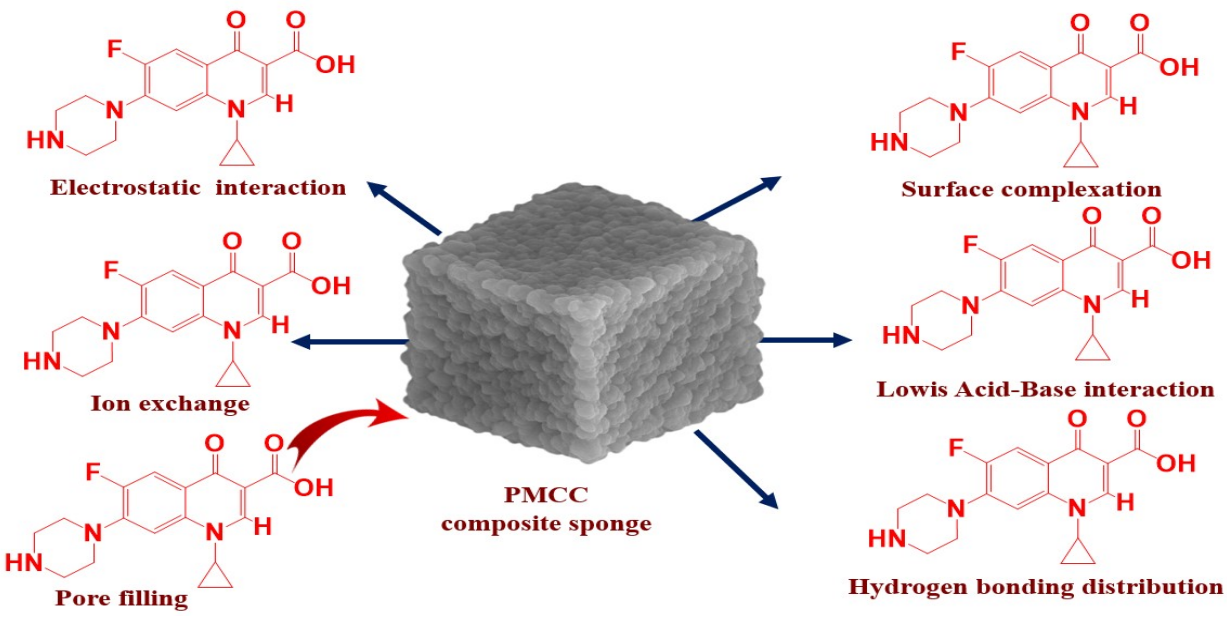

Fig. S2. Mechanism of interaction.

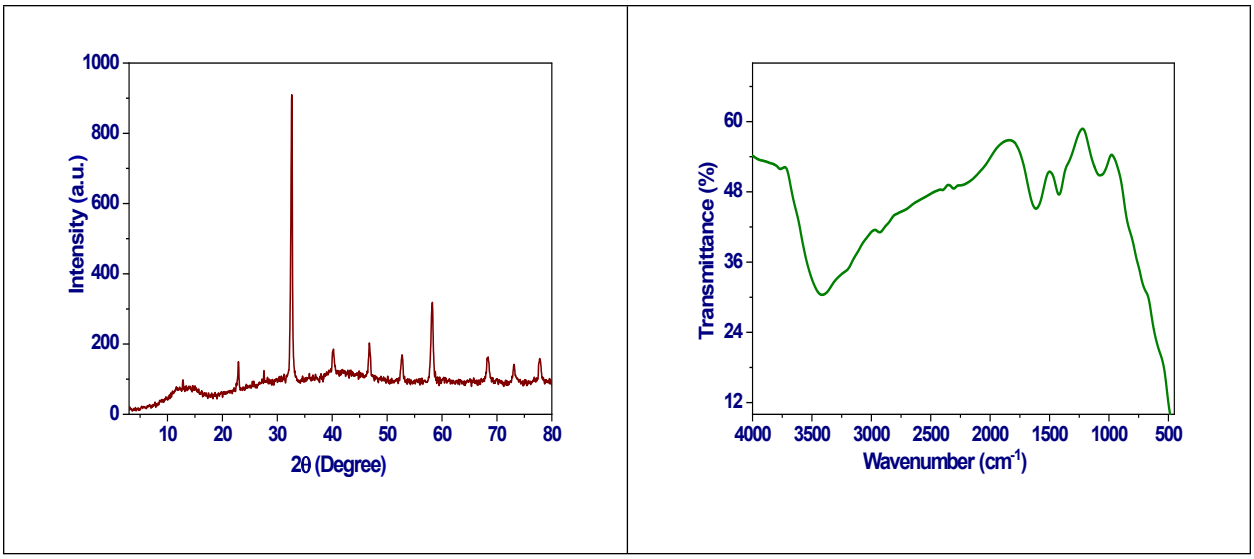

Fig. S3. (a) PXRD of regenerated PMCC, and (b) FT-IR of regenerated PMCC.

References

[1] I. Langmuir, The constitution and fundamental properties of solids and liquids. Part I. Solids, J. Am. Chem. Soc., 38 (1916) 2221-2295.
[2] H.M.F. Freundlich, Over the adsorption in solution, J. Phys. Chem., 57 (1906) 385-471.
[3] M. Dubinin, The equation of the characteristic curve of activated charcoal, Proc. Acad. Sci. USSR Phys. Chem. Sect., 55 (1947) 327-329.
[4] V.P. M.I. Tempkin, Kinetics of ammonia synthesis on promoted iron catalyst, Acta Phys. Chim. USSR, 12 (1940) 327-356.
[5] D.P. Vargas, L. Giraldo, J.C. Moreno-Piraján, CO2 adsorption on activated carbon honeycomb-monoliths: a comparison of Langmuir and Toth models, International journal of molecular sciences, 13 (2012) 8388-8397.
[6] S.K. Lagergren, About the theory of so-called adsorption of soluble substances, Sven. Vetenskapsakad. Handingarl, 24 (1898) 1-39.
[7] Y.-S. Ho, G. McKay, Sorption of dye from aqueous solution by peat, Chemical engineering journal, 70 (1998) 115-124.
[8] W.J. Weber Jr, J.C. Morris, Kinetics of adsorption on carbon from solution, J. Sanit. Eng. Div., 89 (1963) 31-59.
[9] M.H. Dehghani, A. Dehghan, A. Najafpoor, Removing Reactive Red 120 and 196 using chitosan/zeolite composite from aqueous solutions: Kinetics, isotherms, and process optimization, Journal of Industrial and Engineering Chemistry, 51 (2017) 185-195.
[10] E.C. Lima, A. Hosseini-Bandegharaei, J.C. Moreno-Piraján, I. Anastopoulos, A critical review of the estimation of the thermodynamic parameters on adsorption equilibria. Wrong use of equilibrium constant in the Van't Hoof equation for calculation of thermodynamic parameters of adsorption, Journal of molecular liquids, 273 (2019) 425-434.

[11] H.N. Tran, S.-J. You, A. Hosseini-Bandegharaei, H.-P. Chao, Mistakes and inconsistencies regarding adsorption of contaminants from aqueous solutions: a critical review, Water research, 120 (2017) 88-116.
[12] B. Oladipo, E. Govender-Opitz, T.V. Ojumu, Kinetics, thermodynamics, and mechanism of Cu (II) ion sorption by biogenic iron precipitate: using the lens of wastewater treatment to diagnose a typical biohydrometallurgical problem, ACS omega, 6 (2021) 27984-27993.
[13] A.H. Khan, H.A. Aziz, P. Palaniandy, M. Naushad, N. Zouli, Ciprofloxacin adsorption onto CNT loaded pumice: adsorption modelling, kinetics, equilibriums and reusability studies, Journal of Molecular Liquids, 399 (2024) 124388.
[14] Q. Li, H. Li, X. Zong, H. Sun, Y. Liu, Z. Zhan, S. Mei, Y. Qi, Y. Huang, Y. Ye, Highly efficient adsorption of ciprofloxacin from aqueous solutions by waste cation exchange resin-based activated carbons: Performance, mechanism, and theoretical calculation, Science of The Total Environment, 912 (2024) 169534.
[15] F. da Silva Bruckmann, A.C.F.P. Fuhr, L. Zibetti, C.R. Bender, L.F.O. Silva, K. da Boit Martinello, N. Ahmad, S. Mohandoss, G.L. Dotto, Adsorption of ciprofloxacin from aqueous solution and fresh synthetic urine by graphene oxide: Conventional and statistical physics modeling approaches, Chemical Engineering Journal, 487 (2024) 150484.
[16] S.M. Khumalo, B.F. Bakare, S. Rathilal, Single and multicomponent adsorption of amoxicillin, ciprofloxacin, and sulfamethoxazole on chitosan-carbon nanotubes hydrogel beads from aqueous solutions: Kinetics, isotherms, and thermodynamic parameters, Journal of Hazardous Materials Advances, 13 (2024) 100404.
[17] Q. Luo, P. Liu, L. Bi, L. Shi, J. Zhou, F. Fang, Q. Lv, H. Fu, X. Li, J. Li, Selective and efficient removal of ciprofloxacin from water by bimetallic MOF beads: Mechanism quantitative analysis and dynamic adsorption, Separation and Purification Technology, 332 (2024) 125832.
[18] B. Yao, W. Zeng, A. Núñez-Delgado, Y. Zhou, Simultaneous adsorption of ciprofloxacin and Cu2+ using Fe and N co-doped biochar: Competition and selective separation, Waste Management, 168 (2023) 386-395.
[19] A. Guesmi, N.B. Hamadi, W. Abd El-Fattah, A. Subaihi, A.A. Alluhaybi, M.G. El-Desouky, A.A. El-Bindary, Efficient removal of ciprofloxacin in aqueous solutions by magnetic se-MOF embedded within a biopolymer (chitosan/alginate): Adsorptive behavior, mechanism study, and optimization using box-Behnken design, International Journal of Biological Macromolecules, (2025) 144274.
[20] F. Al-Ghazzawi, M.M. Al-Mossawi, A. Al-Shawi, K. Al-Attafi, Synthesis and Carbonization of Core-Shell ZIF-67@ ZIF-90 for Ciprofloxacin and Azithromycin Removal, Bulletin of Chemical Reaction Engineering & Catalysis, (2026) 3.
[21] B. Padhan, W. Ryoo, M. Patel, J.K. Dash, R. Patel, Cutting-edge applications of cellulose-based membranes in drug and organic contaminant removal: recent advances and innovations, Polymers, 16 (2024) 2938.
[22] B. Shagdarova, Y. Zhuikova, A. Il'ina, Adsorbent Materials Based on Modified Chitosan for Purification of Aqueous Media from Pharmaceutical Residues, Primarily Antibiotics, Polymers, 17 (2025) 2601.